INTERFACE SCIENCE 8, 131–140, 2000

Misorientation Dependence of the Grain Boundary Energy in Magnesia

DAVID M. SAYLOR, ADAM MORAWIEC*, BRENT L. ADAMS† AND GREGORY S. ROHRER
Department of Materials Science and Engineering, Carnegie Mellon University, Pittsburgh, Pennsylvania 15213-3890, USA

Abstract. Geometric and crystallographic data obtained from a well annealed magnesia polycrystal have been used to specify the five macroscopic degrees of freedom for 4665 grain boundaries. The results indicate, that for this sample, the five parameter grain boundary character space is fully occupied. A finite series of symmetrized spherical harmonics has been used to approximate the misorientation dependence of the relative grain boundary energy. Best fit coefficients for this series were determined by assuming that the interfacial tensions at each triple junction are balanced. The grain boundary energy function shows Read-Shockley behavior at small misorientations and a broad minimum near the $\Sigma 3$ misorientation. Furthermore, misorientations about the $\langle 100 \rangle$ axis create boundaries with relative energies that are less than those created by misorientations about the $\langle 110 \rangle$ or $\langle 111 \rangle$ axes.

Keywords: grain boundary energy, magnesia, electron backscattered diffraction, triple junctions, atomic force microscopy, thermal grooves

Introduction

In a pure single phase material, the grain boundary character can be specified by the five macroscopic degrees of freedom that define the crystallographic lattice misorientation and the boundary plane. Because the local atomic structure in the intergranular regions of a polycrystal is distinct from the bulk and varies with character, the free energy per unit area of the grain boundary is also expected to vary with character. The number of distinct grain boundary characters that can exist in nature is very large, and this has made it challenging to characterize their diversity and establish character-property correlations. For example, if one considers a cubic material, the number of distinct grain boundaries can be enumerated in the following manner. The three Euler angles ($\phi_1 \Phi \phi_2$) that characterize the misorientation range from zero to 2π, π, and 2π, respectively [1]. The two spherical angles ($\theta\phi$) that characterize the boundary plane range from zero to 2π and π, respectively. Since the boundary normal can be selected in two directions, the crystals can be exchanged, and one can apply 24 cubic symmetry operators to either crystal, there are $2 \cdot 2 \cdot 24^2$ combinations of the five angular parameters that lead to identical bicrystals. Thus, the number of distinct boundaries, N, is:

$$N = \frac{\pi^5}{288\Delta^5}, \tag{1}$$

where Δ is the angular resolution (in radians) with which the degrees of freedom are measured. While this particular parameterization is nonuniform and leads to singularities, it accurately illustrates that for reasonable values of Δ, the number of boundaries is very large. For example, if $\Delta = 0.087$ (5°), there are 2×10^5 distinct boundaries. Furthermore, the number of distinct boundaries increases significantly for smaller values of Δ and is higher for less symmetric crystals.

Until recently, it was not possible to characterize enough grain boundaries to measure the complete anisotropy of the energy or even to know if all of the distinct possibilities are realized in nature. Therefore, previous experimental studies of the grain

*Present address: Instytut Metalurgii i Inzynierii, Materialowej PAN, Reymonta 25, 30-059 Krakow, Poland.
†Present address: Department of Mechanical Engineering, Brigham Young University, 435 CTB, P.O. Box 24201, Provo, Utah 84602-4201, USA.

boundary energy-character relationship in ceramics have focused on one-dimensional slices through the five-dimensional grain boundary character space [2–7]. Larger subsections of the space have been probed by simulation [8]. The objective of this paper is to describe our recent characterization of the five degrees of freedom of 4665 grain boundaries in a magnesia polycrystal equilibrated at 1600°C in air. Based on these data, the relative grain boundary energy is determined as a function of the three misorientation parameters.

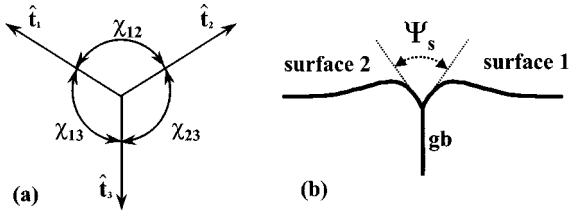

Figure 1. (a) Schematic illustration of an internal triple junction where three grains meet. (b) Schematic illustration of a thermal groove where a grain boundary intersects a free surface.

Experimental

(i) Experimental Approach

Acquisition of the geometric and crystallographic data required to characterize the grain boundary degrees of freedom was accomplished by using a recently developed instrument known as the Mesoscale Interface Mapping System (MIMS) [9]. The MIMS is based on a conventional scanning electron microscope (SEM) that is used in concert with computers that automatically record images, correct dimensional distortions, detect the locations of triple junctions, measure apparent grain boundary dihedral angles, control the beam and sample stage position, and acquire and analyze electron backscattered diffraction patterns (EBSPs). The operation of the MIMS can be briefly described in the following way. The sample surface is divided into sectors and, in each sector, a secondary electron image is recorded and analyzed to reveal the locations of boundaries and triple junctions. Once image distortions have been removed from these data, the grain boundary dihedral angles are determined and the electron beam is directed (in spot mode) to each grain in the sector, where a backscattered electron diffraction pattern is recorded, and the orientation is determined. When the sector characterization is complete, the microscope stage is automatically moved to the next sector. The entire procedure is carried out under computer control and at its conclusion, three orientations and apparent dihedral angles are recorded for each triple junction on the specimen surface. To determine boundary inclination and the true dihedral angles, a thin layer of the sample is removed by polishing and the procedure is repeated.

The condition for local equilibrium at the intersection of two or more interfaces with anisotropic energies was originally articulated by Herring [10]. In the present analysis, we ignore the influence of the grain boundary plane on the energy. In this case, the condition for local equilibrium at a triple junction reduces to the well known Young equation:

$$\sum_i \gamma_i(\Delta\mathbf{g})\hat{t}_i = 0, \tag{2}$$

where γ_i, the energy of the i-th boundary, is assumed to be a function only of the misorientation ($\Delta\mathbf{g}$), and $\hat{t}_i$ is the unit vector tangent to the i-th boundary plane at the triple junction. With respect to the experimental measurements, Eq. (2) can be rewritten in the following way:

$$\sum_i \gamma_i(\Delta\mathbf{g}) \cos \chi_{ij} = 0, \tag{3}$$

where χ_{ij} denotes the angle between vectors $\hat{t}_i$ and $\hat{t}_j$, as shown in Fig. 1(a). In this paper, our approach to determining the energy is to approximate the function $\gamma_i(\Delta\mathbf{g})$ as a finite series of symmetrized spherical harmonics. The unknown coefficients of the series are then determined by fitting the observed data for each triple junction to the condition for local equilibrium given by Eq. (3).

The thermal groove that forms at the intersection of the grain boundary and the sample surface provides an alternative way to measure the energy. If we again assume that the grain boundary plane does not influence the energy, and further assume that the boundary plane is normal to the surface and that the surface energy (γ_s) is isotropic, the condition for local equilibrium can be written in the following way:

$$\frac{\gamma(\Delta\mathbf{g})}{\gamma_s} = 2\cos\left(\frac{\psi_s}{2}\right), \tag{4}$$

where ψ_s is the surface dihedral angle defined in Fig. 1(b). Atomic force microscopy (AFM) has been used to measure ψ_s for thermal grooves at boundaries

with known misorientation. From these measurements, it is possible to independently estimate the relative grain boundary energy and test the validity of the best fit function determined from the analysis of the triple grain boundary junctions.

(ii) Sample Preparation

Magnesia powder was formed by decomposing 99.7% pure magnesium carbonate (Fisher Scientific) at 997°C in air. Uniaxial compaction in a hot press for 2 h at 1700°C and 61 MPa produced a disc with a diameter of 50 mm and an average thickness of 1.5 mm. Specimens cut from the disc were then packed in a magnesia crucible with the parent powder and annealed for 48 h at 1600°C in air. At the end of this treatment, the specimens were translucent. The geometric measurements used to characterize the triple junction geometry require samples that are flat and have two parallel faces. Appropriate surfaces were prepared using an automatic polisher (Logitech PM5). The surfaces were initially lapped parallel with a 9 μm alumina slurry, and the final polish was achieved using an alkaline (pH$\sim$10) colloidal silica (0.05 μm) slurry. The flatness of the final surface was measured using an inductive axial movement gauge head with a resolution of 0.1 μm (Brown and Sharpe, TESR, Model TT22); surfaces were determined to be flat within $\pm$0.3 μm over lateral dimensions of 1 cm. For serial sectioning, the same polisher and gauge head were used to remove thin layers and measure the amount removed, respectively. To enhance the contrast at the grain boundaries, the surface was thermally grooved by annealing it in air for 5 h at 1400°C. The average grain size of the sample was 109 μm. At this stage, one sample was analyzed for impurities. The sample contained 0.2 wt. % Ca, 0.02 wt. % Al, 0.03 wt. % Fe, 0.02 wt. % Si, and 0.03 wt. % Y.

(iii) Orientation and Dihedral Angle Measurements

Crystallite orientations and grain boundary dihedral angles at triple junctions were measured using the MIMS. The MIMS system is integrated with a Phillips XL40 FEG SEM. The uncoated magnesia sample was tilted at 70° for imaging and acquisition of the EBSPs. Each sector was analyzed at a magnification of 200×, which corresponds approximately to a pixel-to-pixel separation of 0.83 μm in the lateral direction and 0.96 μm in the vertical direction. Under these conditions, the error in the calculation of the in-plane angles is estimated to be $\pm$10° for a material with a grain size of $\sim$100 μm. The patterns were indexed using an algorithm previously described by Morawiec [11], which returns a set of Euler rotation angles ($\phi_1 \Phi \phi_2$) relating the crystal reference frame to the sample reference frame. The error in the absolute orientation (**g**) and misorientation (Δ**g**) obtained in this manner are estimated to be $\pm$5° and $\pm$0.5°, respectively.

After the first planar section was characterized, a 6.2 ± 0.3 μm layer was removed by polishing and the entire sample surface was imaged once again. Analysis of the geometric data requires a global coordinate reference for all of the images that is more accurate than the one provided by the stage coordinates. To establish this reference frame, the images in each planar section must be positioned with respect to one another and then the two planar sections must be aligned. To determine the relative positions of the images in a single planar section, we used the following two step procedure. Adjacent images in each planar section are deliberately recorded so that all adjacent sectors overlap; this makes it possible to determine an offset between each neighbor pair by maximizing the contrast correlation in the overlapped region. However, when as many as 100 images in a 10 by 10 array are positioned using only nearest neighbor offsets, significant cumulative errors arise. In other words, if the distance between two points in distant images is computed by summing the nearest neighbor offsets along two different paths through the array of images, the distances usually differ. So, the second step of the image positioning algorithm is to randomly select paths through the image array and reposition the images to minimize the differences between distances computed in the global reference frame and those determined by summing the nearest neighbor offsets along equivalent random paths. The errors associated with positioning the images in this manner were usually less than one pixel.

After all images in both sections had been positioned, triple junctions on the top section were visually linked with the corresponding triple junctions on the bottom section. A total of 1555 triple junctions were characterized in this manner. The sections were then aligned by minimizing the lateral distance between triple junctions on both sections. The alignment procedure is described in detail elsewhere [12]. Using the lateral distances between corresponding junctions and the depth of material removed, the triple line directions were calculated. The triple line directions, along with the in-plane

directions of the grain boundaries, were used to calculate the true dihedral angles.

(iv) Determining the Relative Grain Boundary Energies

Using the experimental techniques described above, it is possible to specify all of the quantities in Eq. (3), except for the grain boundary energies. Unfortunately, for N observed triple junctions, there are 2N independent equilibrium equations and a larger number (with an upper limit of 3N) of unknown energies. Thus, some level of approximation is required. Here, the grain boundary energy is approximated as a finite series of harmonic basis functions which have the symmetry of cubic misorientation space:

$$\gamma(\Delta\mathbf{g}) = \sum_{\ell=1}^{\infty} \sum_{\mu=1}^{M(\ell)} \sum_{\nu=1}^{M(\ell)} C_{\ell\mu\nu}\, \dddot{T}_{\ell}^{\mu\nu}(\Delta\mathbf{g}), \qquad (5)$$

where $\dddot{T}_{\ell}^{\mu\nu}(\Delta\mathbf{g})$ are cubic-cubic symmetric generalized spherical harmonics functions, $C_{\ell\mu\nu}$ are the coefficients of the series, and $M(\ell)$ are the number of linearly independent solutions which are enumerated by the index μ or ν [1]. These cubic-cubic functions can be used to represent any property which is a function of misorientation in a homophase cubic system. Furthermore, knowing that the grain boundary energy function should exhibit certain properties allows us to introduce boundary conditions. In the limit that the misorientation between adjacent grains goes to zero, the energy function must also be zero:

$$\gamma(\mathbf{I}) = 0, \qquad (6)$$

where $\mathbf{I}$ is the identity misorientation. Also, since the energies can only be determined in a relative sense, we have normalized the function such that the average energy is equal to one. Introducing these two conditions leads to the following expression for the grain boundary energy as a function of misorientation:

$$\gamma(\Delta\mathbf{g}) = \left[1 - \dddot{T}_{4}^{11}(\Delta\mathbf{g})\right] + \sum_{\ell=6}^{\infty} \sum_{\mu=1}^{M(\ell)} \sum_{\nu=1}^{M(\ell)} C_{\ell\mu\nu} \left[\dddot{T}_{\ell}^{\mu\nu}(\Delta\mathbf{g}) - \dddot{T}_{\ell}^{\mu\nu}(\mathbf{I})\, \dddot{T}_{4}^{11}(\Delta\mathbf{g})\right]. \qquad (7)$$

After substituting the grain boundary energy (Eq. (7)) into the local equilibrium condition (Eq. (3)), a standard linear least squares procedure was used to determine the best fit values of the coefficients [13]. To assess the quality of the fit, the ratio (α) of the sum of squares of the residuals to the difference between the number of equations and the number of free parameters was computed as a function of the number of terms (coefficients) in the series [14]. Based on this analysis, the addition of coefficients beyond $\ell = 12$ did little to improve the quality of the fit and the series was truncated at this point ($\alpha = 0.12$). By truncating the series at this point, the minimum period of oscillations that can be reproduced is 7.5°, so this should be taken as the resolution of the approximation. The limited resolution is presumably related to the experimental errors, particularly those associated with measuring the dihedral angles, and the neglect of the boundary plane anisotropy.

To test the feasibility of approximating the grain boundary energy as a finite series of harmonic basis functions, we carried out the procedure on a control data set generated from a hypothetical grain boundary energy function. This exercise also allows us to examine artifacts associated with the finite series approximation and the impact of the approximation's limited resolution. We use the Read-Shockley (RS) model [15] for the energy of low angle grain boundaries and assume that high angle boundaries have a constant energy. In this model, the grain boundary energy is a function of a single misorientation parameter, θ_{mis}, which is the angle of misorientation about the rotation axis common to the two grains. The energies of grain boundaries with $\theta_{\text{mis}} \leq 15^\circ$ were assumed to be $\gamma(\theta_{\text{mis}}) = x(1 - \ln(x))$, where $x = \theta_{\text{mis}}/15^\circ$ and θ_{mis} is given in degrees. The energies of boundaries with $\theta_{\text{mis}} > 15^\circ$ are taken to be constant and equal to 1. A set of triple junctions, equal in number to the experimental data set, were generated by assigning Euler angles over the complete domain for all possible orientations using an algorithm that guarantees a random orientation distribution. Using the RS energy model, the dihedral angles at the triple junctions were calculated by solving Eq. (3) with respect to $\cos(\chi_{ij})$ and using these values to calculate χ_{ij}. To account for the experimental errors, the ideal dihedral angles were altered by randomly generated angles ($\Delta\chi$) with a population governed by the von Mises distribution, $\exp(\kappa \cos \Delta\chi)$, with $\kappa = 300$. This distribution is peaked at $\Delta\chi = 0$; values outside the limits of $\pm 10^\circ$ are very unlikely.

A comparison between the RS model and the fit function for the ⟨110⟩ misorientation axis is shown in

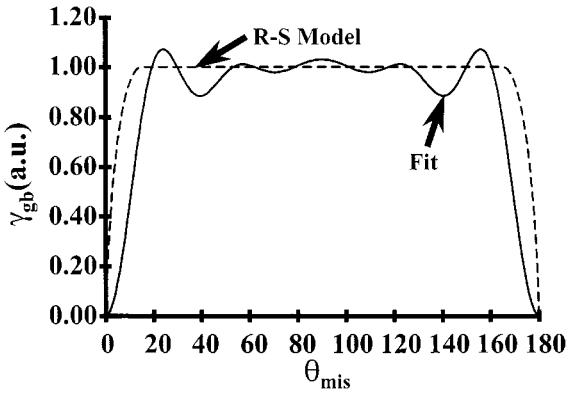

Figure 2. Comparison of a model grain boundary energy function and an approximate function fit to a data set generated from the RS model.

Fig. 2. The fit function shows the same general trends as the model; it increases as the misorientation angle increases from zero to an angle of $\sim 20^\circ$. For misorientation angles $>20^\circ$, the function flattens and oscillates around 1. However, the exact shape of the RS model is not reproduced by the approximate function, especially near the origin. Instead of a sharp cusp at zero misorientation and a constant energy value of one for misorientations greater than the limiting angle, the slope of the function vanishes at zero misorientation and there are oscillations (± 0.12) about one for the higher angle misorientations. This is an unavoidable consequence of approximating the energy as a finite series of harmonic functions. While adding additional terms to the series can improve the approximation if a larger set of data were available, these characteristic features will, to some extent, persist as long as this particular set of basis functions is used.

(v) Thermal Groove Measurements

The surface dihedral angles of 184 thermal grooves were measured by AFM and the misorientation across the boundaries was determined from EBSPs. Using these data, the relative grain boundary energy was calculated according to Eq. (4). These measurements were conducted using a previously described procedure [16].

Results

We have characterized all five degrees of freedom for 4665 grain boundaries and use the following scheme for the representation of these data: a three-dimensional space is used to represent the misorientation parameters and, for each misorientation in this space, the two boundary plane parameters are represented on an inverse pole figure. Here, we use Rodrigues-Frank (RF) space to represent the misorientations [17]. Because of cubic-cubic misorientation symmetry, there are $2 \cdot 24 \cdot 24$ equivalent rotations corresponding to any given misorientation. We select a rotation with the smallest misorientation angle (sometimes called the disorientation). However, since there are 48 equivalent rotations with the minimum misorientation, we select the one whose axis lies in a fundamental zone; here we define the fundamental zone as the region of RF space where is the misorientation angle is minimum and the axis $\langle uvw \rangle$ lies in the standard streographic triangle such that $u \geq v \geq w \geq 0$. Thus, each misorientation can be represented by a vector ($\vec{R}$) in RF space that is parallel to an equivalent misorientation axis in the fundamental zone and has a length related to the minimum misorientation angle (θ_d) by $|\vec{R}| = \tan(\theta_d/2)$. The perpendicular components of $\vec{R}$ are aligned parallel to the cube axes such that R_1 is parallel to [100]. The three-dimensional fundamental zone of misorientation space is plotted in planar sections perpendicular to R_3 ([001]) and, in Fig. 3, the endpoint of each vector is indicated by a point on the plot. According to these data, misorientation space is completely populated. However, note that many of the data are superimposed so it is incorrect to assume that Fig. 3 gives an accurate representation of the population density.

In any particular volume of misorientation space that we assume contains effectively equivalent misorientations, we can plot the boundary plane normals on an inverse pole figure, as in Fig. 4. To account for the inversion symmetry of the boundary plane, normal vectors pointing in the negative direction were inverted. Furthermore, to avoid any biasing of our description of the boundary plane by arbitrarily selecting one of the two crystallites as the reference frame, one normal vector is plotted for each reference frame. Thus, each boundary creates two points on the inverse pole figure. Figure 4(a) shows an equal area projection of the distribution of boundary planes for all grain boundaries with a misorientation within 8.66° (Brandon's criterion [18]) of the $\Sigma 3$ misorientation. The $\Sigma 3$ misorientation is a 60° rotation about [111]; in RF space this corresponds to a vector with components $R_1 = 1/3$, $R_2 = 1/3$, and $R_3 = 1/3$. For comparison, Fig. 4(b) shows the distribution of boundary planes for misorientations within 5° of a point within the fundamental zone ($R_1 = 0.3$,

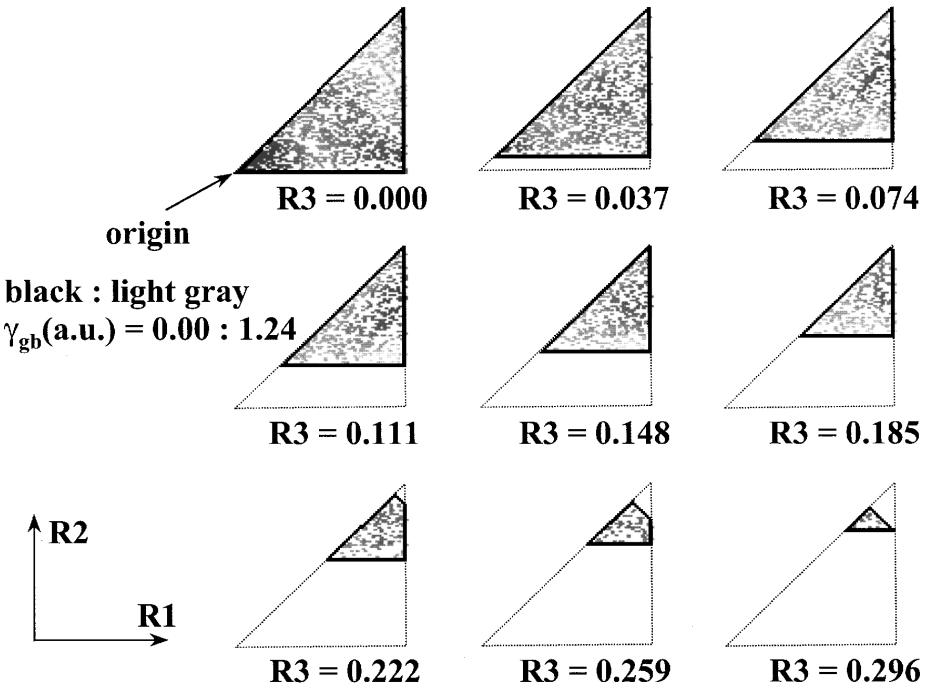

Figure 3. Observed misorientations in a MgO polycrystal. 4665 misorientations are plotted in nine parallel sections of the fundamental zone in RF space. The data points are shaded according to the value of the approximate grain boundary energy function at that misorientation. Black indicates the zero of energy. The highest value, 1.24, is indicated by the lightest shade of gray.

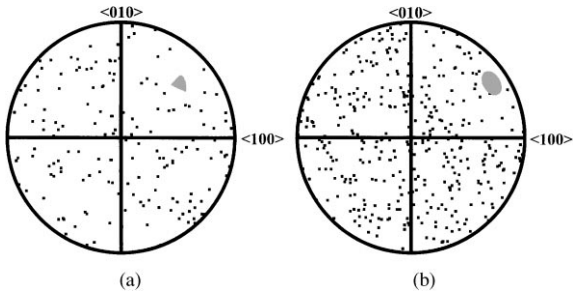

Figure 4. Equal area projection inverse pole figures showing the distribution of boundary planes for (a) grain boundaries with a misorientation within 8.66° of the Σ3 misorientation, $R_1 = 1/3, R_2 = 1/3, R_3 = 1/3$, and (b) grain boundaries with misorientations within 5° of $R_1 = 0.3$, $R_2 = 0.2$, $R_3 = 0.1$. The gray areas show the orientations of the misorientation axes of boundaries included in each projection.

$R_2 = 0.2$, and $R_3 = 0.1$) that is not near a special misorientation. This apparently random distribution is characteristic of most points in disorientation space.

The best fit coefficients for the series in Eq. (7) for $\ell = 12$ are listed in Table 1. Based on these values, we have calculated the value of the function $\gamma_{gb}(\Delta\mathbf{g})$ at each of the observed misorientations. Each point representing a misorientation in Fig. 3 is shaded according to its relative energy, with black corresponding to zero and the lightest gray corresponding to 1.24. Figure 5 shows the functional dependence of the relative grain boundary energy for rotations around the ⟨100⟩, ⟨110⟩, and ⟨111⟩ axes. For comparison, the fit to the RS model

Table 1. Coefficients for the best fit grain boundary energy function.

Coefficient	Value
$C_{6\,1\,1}$	−0.168
$C_{8\,1\,1}$	−0.150
$C_{9\,1\,1}$	0.248
$C_{10\,1\,1}$	−0.113
$C_{12\,1\,1}$	−0.240
$C_{12\,1\,2}$	0.705
$C_{12\,2\,1}$	−0.653
$C_{12\,2\,2}$	−0.364

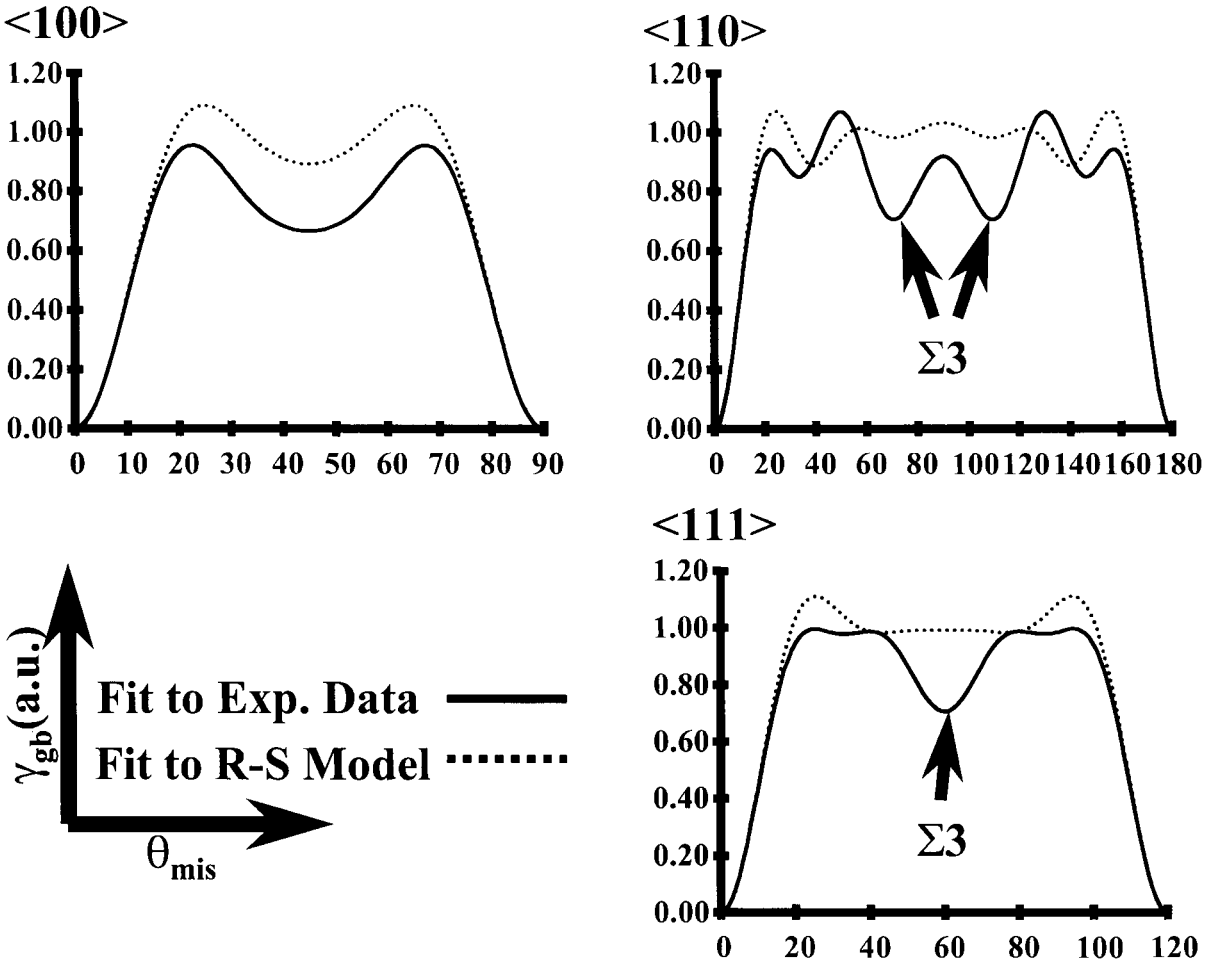

Figure 5. Plots of the approximate grain boundary energy function along three low index axes. For each of the fixed axes, the fit to the model data set generated on the basis of the RS model is included for comparison. The axes in the lower left correspond to each of the three graphs.

is shown on the same plots so that the magnitude of the variations can be compared to the known artifacts in the fit to the model data. There are two obvious differences between the fit to the experimental data and the fit to the model data. The fit to the experimental data shows a broad minimum at the $\Sigma 3$ misorientation and a reduced average energy for rotations about the $\langle 100 \rangle$ axis.

The AFM measurements yielded an average value of $\gamma(\Delta \mathbf{g})/\gamma_s$ of 1.08, with maximum and minimum $\gamma(\Delta \mathbf{g})/\gamma_s$ values of 1.60 and 0.48, respectively. Figure 6 shows the variation of $\gamma(\Delta \mathbf{g})/\gamma_s$ with the smallest symmetrically equivalent misorientation angle between the bounding grains. Low angle boundaries ($<10^\circ$) have relatively lower values of $\gamma(\Delta \mathbf{g})/\gamma_s$. The data set was probed to determine the values of $\gamma(\Delta \mathbf{g})/\gamma_s$ for boundaries with misorientations within Brandon's criterion [18] (limiting angle $= 15^\circ$) of low Σ CSL misorientations ($\Sigma \leq 9$). The average values for $\gamma(\Delta \mathbf{g})/\gamma_s$ at these misorientations are listed in Table 2. Only $\Sigma 3$ has an average $\gamma(\Delta \mathbf{g})/\gamma_s$ value significantly below the average of the distribution of the entire data set.

Table 2. $\gamma(\Delta \mathbf{g})/\gamma_s$ for special boundaries.

Σ	$\gamma(\Delta \mathbf{g})/\gamma_s$
3	0.63
5	1.14
7	1.05
9	1.13

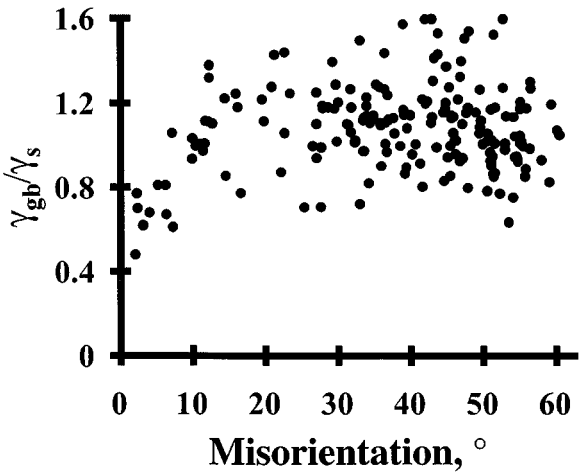

Figure 6. Plot of $\gamma(\Delta\mathbf{g})/\gamma_s$, determined based on AFM measurements of 184 randomly selected thermal grooves. The horizontal axis is the minimum misorientation angle.

Discussion

Having measured the character of 4665 boundaries, we are now in a position to comment on the natural distribution of boundaries over the five parameter space. While Fig. 3 shows that all regions in the fundamental zone of misorientation space are populated, the distribution of misorientations is not consistent with an ideal random misorientation distribution [19, 20]. In fact, our analysis of the misorientations indicates that the sample exhibits a higher than normal fraction of low angle grain boundaries. The orientations themselves show a weak ⟨111⟩ fiber texture that is 2.1 times random. The distribution of boundary planes (see Fig. 4) for a given misorientation appears to be largely random. There is, however, one interesting point regarding the distribution of planes near the Σ3 misorientation: few boundaries are made up of {111} planes. This might be related to the polar character of the {111} plane and its relatively higher energy [21].

Grain boundary studies have traditionally focused on special coincident site lattice (CSL) boundaries. Therefore, it is useful to characterize our observations with respect to this model. CSL boundaries occur when the misorientation between adjacent crystallites permits (with the appropriate translation) some fraction of the lattice sites from the two grains to coincide; CSL boundaries are named by a Σ number, which is the inverse of the fractional number of coincident sites. In the sample we examined, fewer than 10% of all of the boundaries are associated with a high coincidence ($\Sigma \leq 9$) misorientation (see Table 3). Of the CSL boundaries that we did observe, the populations are generally within a factor of two of what one would expect based on a completely random distribution [22]. The only exception was the population of Σ1 boundaries, which make up 4.8% of the data set.

Table 3. Population of special boundaries in a MgO polycrystal.

Boundary	Population in present data[a] (%)	Expected in a random population[b] (%)
Σ1	4.8	1.98
Σ3	1.8	1.53
Σ5	1.5	1.07
Σ7	0.45	0.86
Σ9	0.86	0.88

[a]Within Brandon's criterion, assuming a cutoff of 15°.
[b]From Ref. 22.

The energies of the low angle boundaries increased from zero at zero misorientation to an approximately constant value after 20°. This behavior is consistent with both the RS model and with previous observations of MgO and NiO bicrystals [2–5]. The relatively lower energies of the low angle grain boundaries in this sample were verified independently by the thermal groove measurements. In Fig. 6, boundaries with low angles of misorientation have a lower relative energy, and as the misorientation angle increases, the $\gamma(\Delta\mathbf{g})/\gamma_s$ values become a constant band with a significant amount of scatter.

The coincidence site lattice (CSL) model predicts that grain boundary energy scales with the fraction of lattice sites in the adjacent crystallites that coincide in the boundary plane. The validity of this model has been demonstrated in a number of previous studies. Most relevant to the current work, we note that Kimura et al. [5] and Dhalenne et al. [3, 4] demonstrated that the energies of ⟨110⟩ symmetric tilt boundaries with a high degree of coincidence were relatively lower than those that did not. However, one must exercise caution when assuming a link between lattice coincidence and grain boundary energy. While the fractional lattice coincidence is determined by the misorientation alone, it is only for certain special boundary planes that the atoms in the intergranular region occupy coincident positions. For other planes separating crystallites of the same misorientation, there is no reason to anticipate that the energy should scale with the lattice coincidence. For example, rotations of 70.53° and 109.47° about [110] are both Σ3 misorientations; however, a high degree of

coincidence in the intergranular region occurs only for symmetric {111} boundary planes. This configuration is realized by a symmetric 70.53° rotation, but not for the symmetric 109.47° rotation. The previous bicrystal studies both demonstrate the significant effect of the boundary plane on the boundary energy. In the case of MgO, the energy of 109.47° Σ3 rotation was approximately 40% higher than the 70.53° Σ3 rotation [5]. The effect was even larger in the NiO case where the energy of the 109.47° Σ3 rotation was 300% higher than the 70.53° Σ3 rotation [4]. In the current study, we are averaging over all possible boundary planes and because the special planes constitute an insignificant part of the population, it does not necessarily follow that we should expect boundaries with these misorientations to have relatively lower energies. Furthermore, we should point out that when all five degrees of freedom of the grain boundary character are determined, those highly symmetric boundaries with high coincidence are extraordinarily rare in a random polycrystal and, therefore, are of questionable significance.

In spite of the fact that we are averaging over all boundary planes, the relative energy at the Σ3 misorientation is significantly lower than most other places in misorientation space. The value of the best fit function at this point falls below the oscillations produced by the same fit to the RS model. The conclusion that boundaries with this misorientation have lower energy is verified by the thermal groove data, which also show a minimum at Σ3. It should be noted that the shape of the minimum at this point is not likely to be accurate. Considering the characteristics of the basis functions, we do not expect to resolve narrow cusps in the energy function (narrower than the resolution limit of the function) and we also expect any cusps that are resolved to be approximated as broad minima. Along the low index rotation axes, there are additional local minima in the best fit function (see Fig. 5). However, when we consider the results of the fit to the model data set (see Fig. 3), the shallow local minima in our best fit function must be attributed to the characteristics of the harmonic series rather than the sample.

Another characteristic feature of the approximate energy function is that the energy of boundaries with rotations about the ⟨100⟩ axis are significantly lower than those about the ⟨110⟩ and ⟨111⟩ axes. This characteristic is consistent with the previous bicrystal studies of MgO and NiO which show that ⟨100⟩ twist boundaries have lower energy on average than ⟨110⟩ tilt boundaries [3–5]. Again, we note that the energy function derived in the present paper averages over grain boundary planes while the bicrystal studies were carried out on a subset of special boundary planes.

The approximate $\gamma_{gb}(\Delta\mathbf{g})$ function also exhibits a broad minimum (at $\vec{R} = \langle 0.4142, 0.2071, 0.074\rangle$) that is not associated with any low CSL misorientations. At this point in misorientation space, the energy is approximately 60% of the average energy for all other boundaries. This minimum was not reproduced by the thermal groove measurements where the average $\gamma(\Delta\mathbf{g})/\gamma_s$ value for misorientations within 10° of the minimum (1.11) was approximately the same as the average value for the entire data set (1.09). It is unlikely that the anisotropy of γ_s, which is about 7% at 1400°C, could result in such a large deviation between the measurement techniques [21]. It is also unlikely that the measurement errors associated with either of the techniques, which are assumed to be normally distributed, could be responsible for the large differences. One possible explanation for the minimum is that it is an artifact of the oscillatory basis functions that we have used to approximate the grain boundary energy function.

In this paper, the grain boundary energy of MgO is presented as a function of three misorientation variables. Thus, each point in misorientation space represents the entire range of boundary planes that are specified by the remaining two neglected parameters. However, it is not appropriate to consider the energy to be an average over the possible planes, since by ignoring these two variables, we also neglect the differential terms in the Herring [11] condition for local equilibrium (the so-called torque terms). The torque terms account for the tendency of a boundary to rotate to a plane of minimum energy. They are, therefore, an important factor that determines the geometry of the triple junction. Past studies of thermal grooves have illustrated that the differential terms acting normal to the boundary plane can have a magnitude that is similar to the interfacial tensions [21]. We estimate that to evaluate the grain boundary energy function over all five macroscopic degrees of freedom, it will be necessary to characterize approximately 10^5 triple junctions. Recent improvements in the MIMS suggest that it will soon be possible to collect a data set of this size, and recent advances in the analysis of five parameter data sets suggest that it will be possible to derive the grain boundary energy from such observations [23]. These improvements are expected to lead to a more reliable approximation for the grain boundary energy

with greater resolution over the entire space of macroscopic grain boundary parameters.

Conclusion

Characterization of 4665 grain boundaries in a well annealed magnesia polycrystal indicates that the five parameter grain boundary character space is fully occupied. A finite series of symmetrized spherical harmonics has been used to approximate the misorientation dependence of the relative grain boundary energy. The grain boundary energy function shows Read-Shockley behavior at small misorientations and a broad minimum near the $\Sigma 3$ misorientation. Furthermore, misorientations about the $\langle 100 \rangle$ axis create boundaries with relative energies that are less than those created by misorientations about the $\langle 110 \rangle$ or $\langle 111 \rangle$ axes.

Acknowledgment

This work was supported primarily by the MRSEC Program of the National Science Foundation under Award Number DMR-9632556.

References

1. H.-J. Bunge, *Texture Analysis in Materials Science*, translated by P.R. Morris (Butterworths, London, 1982).
2. D.W. Readey and R.E. Jech, J. Amer. Ceram. Soc. **51**, 201 (1968).
3. G. Dhalenne, A. Revcolevschi, and A. Gervais, Phys. Stat. Sol (a) **56**, 267 (1979).
4. G. Dhalenne, M. Déchamps, and A. Revcolevschi, J. Amer. Ceram. Soc. **65**, C11 (1982).
5. S. Kimura, E. Yasuda, and M. Sakaki, Yogyo-Kyokai-Shi **94**, 795 (1986).
6. D.M. Duffy and P.W. Tasker, Phil. Mag. **A47**, 817 (1983).
7. D.M. Duffy and P.W. Tasker, Phil. Mag. **A48**, 155 (1983).
8. D. Wolf, J. Mater. Res. **5**, 1708 (1990).
9. C.T. Wu, B.L. Adams, C.L. Bauer, D. Casasent, A. Morawiec, S. Ozdemir, and A. Talukder, Ultramicroscopy, in press.
10. C. Herring, in *The Physics of Powder Metallurgy*, edited by W.E. Kingston (McGraw Hill, New York, 1951), p. 143.
11. A. Morawiec, J. Appl. Cryst. **32**, 788 (1999).
12. A. Morawiec and D. Saylor, in *Proc. of the Twelfth International Conference on Textures of Materials*, edited by J. Szpunar (NRC Research Press, Ottawa, 1999), p. 198.
13. W.H. Press, B.P. Flannery, S.A. Teukolsky, and W.T. Vetterling, *Nurmerical Recipes in Pascal* (Cambridge University Press, Cambridge, 1989).
14. G.E. Forsythe, J. Soc. Ind. Appl. Math. **5**, 74 (1957).
15. W.T. Read and W. Shockley, Phys. Rev. **78**, 275 (1950).
16. D.M. Saylor and G.S. Rohrer, J. Am. Ceram. Soc. **82**, 1529 (1999).
17. F.C. Frank, Met. Trans. **19A**, 403 (1988).
18. D.G. Brandon, Acta Met. **14**, 1479 (1966).
19. A. Morawiec, J. Appl. Cryst. **28**, 289 (1995).
20. A. Morawiec, J. Appl. Cryst. **29**, 164 (1996).
21. D.M. Saylor, D.E. Mason, and G.S. Rohrer, J. Am. Ceram. Soc. **83**, 1226 (2000).
22. D.H. Warrington and M. Boon, Acta Met. **23**, 599 (1975).
23. A. Morawiec, Acta Mater. **48**, 3525 (2000).